



Superhydrophobic polyvinylidene fluoride/polyimide nanofiber composite aerogels for thermal insulation under extremely humid and hot environment

Fan Yang¹, Xingyu Zhao¹, Tiantian Xue¹, Shijia Yuan¹, Yunpeng Huang², Wei Fan^{1*} and Tianxi Liu^{1,2*}

ABSTRACT Excellent thermal insulating materials are highly demanded in various applications including buildings, aerospace and sport equipment. However, in practical applications, the performance of thermal insulating materials usually deteriorates under diverse temperature and humidity conditions. Therefore, it is highly essential to construct a bulk material that exhibits outstanding thermal insulation performance under extremely humid and hot environment. In this work, we have conceived a green and effective strategy to fabricate a superhydrophobic and compressible polyvinylidene fluoride/polyimide (PVDF/PI) nanofiber composite aerogel *via* electrospinning and freeze-drying technique. Interestingly, the PVDF nanofibers and PI nanofibers function as the hydrophobic fibrous framework and mechanical support skeleton, respectively, forming a robust three-dimensional framework with good mechanical flexibility. The PVDF/PI aerogel possesses outstanding superhydrophobic feature (water contact angle of 152°) and low thermal conductivity (31.0 mW m⁻¹ K⁻¹) at room temperature. Significantly, even at 100% relative humidity (80°C), the PVDF/PI aerogel still exhibits a low thermal conductivity of only 48.6 mW m⁻¹ K⁻¹, which outperforms the majority of commercial thermal insulating materials. Therefore, the novel PVDF/PI aerogel is promising as an excellent thermal insulating material for the applications in high-temperature and humid environment.

Keywords: nanofiber aerogel, polyimide, polyvinylidene fluoride, superhydrophobic, thermal insulation

INTRODUCTION

Energy consumption has been a crucial universal issue

due to the rapid industrial development and reduction of fossil energy [1,2]. Thermal insulation is one of the effective ways to decrease energy loss and improve global energy efficiency [3–5]. Excellent thermal insulating materials can find demand in various applications including buildings, aerospace and sport equipment [6,7]. More importantly, the thermal insulating behavior should be stable when materials are exposed outdoor under variable temperature and humid circumstances. However, in practical applications, the performance of thermal insulating materials usually deteriorates under diverse temperature and humidity conditions. For instance, conventional thermal insulating materials, such as polyurethane (PU) and expanded polystyrene (PS), show inferior thermal stability at elevated temperature. On the other hand, the thermal insulating properties of materials are generally compromised when exposed to high humidity environments since water is a highly thermal conductive substance [8,9]. The higher humidity air (i.e., the water molecule) diffusing into the materials would weaken the thermal insulation performance and even destroy the structure of the samples. Therefore, it is highly essential to construct a bulk material that exhibits outstanding thermal stability while maintaining good moisture resistance for thermal insulation under extremely humid and hot environment.

Aerogels are porous materials with nanostructures and exhibit promising potential for heat management due to their high porosity, low density, large specific surface area and low thermal conductivity [10–14]. In the past few decades, a variety of aerogel materials have been suc-

¹ State Key Laboratory for Modification of Chemical Fibers and Polymer Materials, College of Materials Science and Engineering, Innovation Center for Textile Science and Technology, Donghua University, Shanghai 201620, China

² Key Laboratory of Synthetic and Biological Colloids, Ministry of Education, School of Chemical and Material Engineering, Jiangnan University, Wuxi 214122, China

* Corresponding authors (emails: weifan@dhu.edu.cn (Fan W); txliu@fudan.edu.cn or txliu@dhu.edu.cn (Liu T))

cessfully prepared, including graphene [15–17], silica [18], carbon nanotubes [19,20] and synthetic polymers [21,22]. Recently, aerogels based on SiO₂ have become promising thermal insulating materials owing to their ultra-low thermal conductivity [23]. However, brittleness and hygroscopicity as well as processing complexity limit their further development [24]. Polymer aerogels fabricated by the traditional sol-gel process possess good mechanical properties, but they usually have poor thermal stability when used at elevated temperature. More recently, novel nanofiber aerogels derived from polymeric electrospun nanofibers with three-dimensional (3D) interconnected fibrous network have attracted extensive attention [25–27]. On account of their high porosity, low density, high flexibility and elasticity, nanofiber aerogels show great potential as next-generation flexible thermal insulating materials.

In natural structures, the introduction of continuous fibrous structures has been shown to greatly improve material utilization and performance. For example, spider webs draw wide attention for their high specific strength and toughness [28]. Researchers have found that there are stable crosslinking points between the azelons, which make the spider web a stable 2D structure. As advanced fiber materials, electrospun nanofibers show great promise as a remarkable nanoscale building block for nanofiber aerogels due to their prominent flexibility, low density, strong mechanical strength and high aspect ratio [29–31]. Hence, constructing nanofibers into 3D nanofiber aerogels may be an eminent strategy for achieving promising properties in a wide range of applications. At present, many polymers, such as polyacrylonitrile (PAN) [25], poly(vinyl alcohol) (PVA) [32] and polyamide-imide (PAI) [33], have been electrospun into nanofibers for the manufacture of 3D nanofiber aerogels. For instance, polyimide (PI) nanofibers have recently been employed as building blocks and fabricated into nanofiber aerogels due to their excellent mechanical strength, flexibility, thermostability and solvent resistance [34,35]. The prepared PI nanofiber aerogels have displayed great potential for outstanding thermal insulating materials. However, a challenge for PI nanofiber aerogels is their inferior hydrophobicity. In practical applications, especially in high-humidity environment, water will intrude into the aerogels to weaken their thermal insulation property and even destroy 3D structures. Therefore, designing superhydrophobic 3D nanofiber aerogels with excellent structure stability and thermal insulation performance under high-humidity is of great importance.

In this work, we present a strategy of compositing

electrospun polyvinylidene fluoride (PVDF) nanofibers and PI nanofibers to construct 3D nanofiber aerogels with excellent thermal insulation performance under varied temperatures and relative humidity (RH). PVDF nanofibers were selected to build the hydrophobic fibrous framework on account of their rich fluorine-containing segments, while PI nanofibers can provide aerogels with desirable structure and thermal stability. Specifically, superhydrophobic and compressible PVDF/PI nanofiber composite aerogels with an open-cell geometry that consists of bonded nanofibers have been fabricated by freeze-drying method. The resulting PVDF/PI aerogel exhibits high porosity, low density and good mechanical property. More importantly, the PVDF/PI aerogel shows brilliant thermal insulation properties in extremely humid (100% RH) and hot (300°C) environment. Besides, freeze-drying is a simple and cost-effective technique for creating a porous material, and the whole preparing process uses only water as a solvent, which greatly reduces environmental contamination. Therefore, as a novel thermal insulating material, the PVDF/PI aerogel shows promising applications in the field of thermal insulation for buildings and outdoor activities.

EXPERIMENTAL SECTION

Materials

PVDF with a molecular weight of 800,000–900,000 was purchased commercially from Dongguan East Plastic Trade Co., Ltd. 4,4'-Oxidianiline (ODA), pyromellitic dianhydride (PMDA), trichloromethane, *N,N*-dimethylacetamide (DMAc), *N,N*-dimethylformamide (DMF), anhydrous magnesium sulfate and aniline were obtained from Sinopharm Chemical Reagent Co., Ltd. Sodium hydroxide was purchased from Shanghai Titan Scientific Co., Ltd. Bisphenol-A was purchased from Tokyo Chemical Industry Co., Ltd. Paraformaldehyde was bought from Alfa Aesar Chemical Co., Ltd. All chemicals were used as received without further purification. Deionized water was used in all experiments.

Preparation of PVDF nanofibers

Typically, PVDF was dissolved in DMF in an oil bath (~50°C) by magnetic stirring for 24 h to obtain a 15 wt% transparent solution. For electrospinning, the PVDF dispersion was placed in a 10-mL syringe with a spinning nozzle of 0.5 mm inner diameter. The solution feeding rate was 0.04–0.08 mm min⁻¹ and the voltage was 13–17 kV. The obtained electrospun nanofibers were dried in an oven at 70°C for 14 h to remove the residual solvent.

Preparation of PI nanofibers

Polyamic acid (PAA) was synthesized using ODA and PMDA according to our previous work [36]. Briefly, ODA (4.0048 g, 0.02 mol) and 50 mL DMAc were added into a three-necked flask and magnetically stirred at 300 rpm until ODA was completely dissolved. Then, equal molar ratio of PMDA (4.4278 g, 0.02 mol) was added to the reaction system, and the mixture was stirred under 0°C for 3 h to obtain a faint yellow viscous precursor solution. Then, PAA nanofibers were prepared using the same electrospinning parameters as PVDF nanofibers. Afterwards, the resultant PAA nanofibers were thermally imidized by the following process to obtain PI nanofibers: (1) heating to 150°C (1.5°C min⁻¹) and annealing at 150°C for 30 min; (2) heating to 350°C (1.5°C min⁻¹) and annealing at 350°C for 1 h; and (3) cooling down to room temperature.

Synthesis of benzoxazine (BA-a)

BA-a was synthesized using bisphenol-A, paraformaldehyde and amine *via* the Mannich reaction. Bisphenol-A (30 g, 0.13 mol), aniline (24.48 g, 0.26 mol), and paraformaldehyde (15.78 g, 0.53 mol) were added into a three-necked flask under magnetic stirring for 30 min in nitrogen atmosphere. Then the temperature was gradually increased to 110°C. After reaction for 4 h, the mixture was cooled down to room temperature and dissolved in 100 mL of trichloromethane. The obtained solution was washed three times with 2 wt% sodium hydroxide and deionized water successively. Finally, it was processed with anhydrous magnesium sulfate, filtered, and dried at 50°C for 5 h to obtain pale yellow BA-a powders.

Fabrication of PVDF/PI aerogel by freeze-drying method

A certain amount of PVDF nanofibers and PI nanofibers with different mass ratios were dispersed in deionized water (30 mL) by a homogenizer (IKA T25) at 15,000 rpm for 30 min. Subsequently, BA-a (100 mg, as crosslinking agent) powders were added to the dispersion with further homogenization for 20 min to form uniform fiber dispersions. The obtained dispersions were transferred to the desired mold, frozen in liquid nitrogen and then freeze-dried using a freeze-dryer (Labconco Free-Zone freeze-drying system) for 72 h to obtain the uncrosslinked nanofiber aerogel. Eventually, the obtained aerogel was heated at 180°C in nitrogen atmosphere for 1 h to give rise to the crosslinked PVDF/PI aerogel. Other nanofiber composite aerogels were produced by adjusting the ratio of PVDF nanofibers to PI nanofibers for comparison.

Characterizations

The morphologies of the samples were observed by an field emission scanning electron microscope (FE-SEM, S-4800, Japan). Contact angle goniometer (OCA40 Micro, Germany) was used to measure the water contact angles of aerogels. Thermogravimetric analysis was studied on a Netzsch TG 209 F1 Libra under air atmosphere from 100 to 600°C with a heating rate of 10°C min⁻¹. The thermal conductivity of the samples was measured by a hot disk instrument (TPS 2500s, Sweden). All thermal infrared images were obtained by an infrared camera (FOTRIC 226s, USA). The compression experiments and cyclic compression experiments were tested on a universal testing machine (SANS UTM2102, China) with 50-N load cells at a compression rate of 10 mm min⁻¹. Fourier transform infrared spectra (FT-IR) were obtained using an FT-IR spectrometer (Nicolet 8700, USA) in a range of 4,000–400 cm⁻¹. Differential scanning calorimetry (DSC) measurements were collected on a differential scanning calorimeter (DSC-822, Sweden). Humidity was controlled by temperature and humidity test chamber (RTH-80-70, Shanghai Rece Instrument Technology Co., Ltd.). The porosity (P) of the aerogel can be calculated according to Equation (1):

$$P = \left(1 - \frac{\rho_0}{\rho}\right) \times 100\%, \quad (1)$$

where P is the porosity, ρ_0 is the apparent density of the aerogel, and ρ is the density of polymer in bulk state, which is estimated from the weighted average of densities of PVDF (1.75 g cm⁻³) and PI (1.38 g cm⁻³).

RESULTS AND DISCUSSION

The schematic illustration for the preparation of superhydrophobic PVDF/PI nanofiber composite aerogel is shown in Fig. 1a. The corresponding digital photos of the fabrication process are also shown in Fig. S1a. The fabrication of superhydrophobic aerogels began with the electrospinning of PVDF and PI nanofiber membranes. The two prepared flexible nanofiber membranes and BA-a were homogenized in deionized water to obtain a homogeneous nanofiber dispersion, which was then frozen and freeze-dried to get the pre-aerogel. As shown in Fig. S1b and c, nanofibers are well dispersed by homogenizing. However, the pre-aerogel could not self-assemble into a stable aerogel because of weak interaction between nanofibers. Hence, to bring about robust bonding among the nanofibers, the obtained pre-aerogels were further heated at 180°C for 1 h to build crosslinked 3D networks. Fourier transform infrared spectroscopy con-

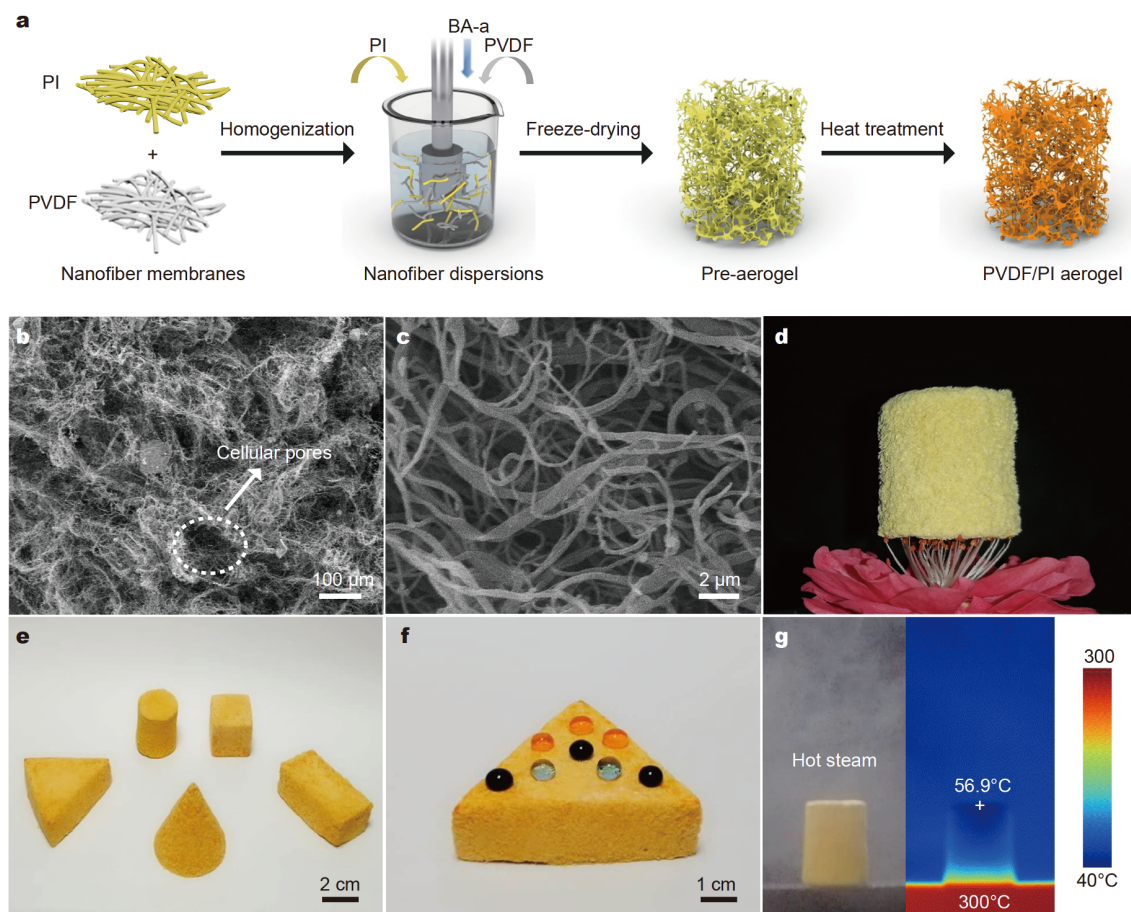


Figure 1 Preparation and structural characterization of the PVDF/PI aerogel. (a) Schematic illustration of the synthetic steps. (b, c) SEM images of the PVDF/PI aerogel. (d) The digital image of PVDF/PI aerogel placed on the top of stamen. (e) Photographs of the PVDF/PI aerogel with different shapes and (f) water droplets on surface of the PVDF/PI aerogel. (g) Digital and thermal infrared images of the PVDF/PI aerogel in high-temperature and humid environment. Left is a digital image, and right is the corresponding thermal infrared images.

firmed the successful synthesis of BA-a (Fig. S2a). During this process, BA-a melted to tightly bond the nanofibers (the melting point of BA-a is about 146°C as shown in Fig. S2b), endowing the resultant aerogels with good structural formability and mechanical properties. As comparison, uncrosslinked aerogels without BA-a as crosslinking agent exhibit poor mechanical stability (Fig. S3). In addition, the mass ratio of PVDF nanofibers to PI nanofibers was investigated to obtain composite aerogels with the optimal performance. As shown in Fig. S4, the PVDF/PI aerogel with mass ratio of 3:1 exhibits the optimized density, thermal conductivity and mechanical property. Therefore, unless specifically noted, PVDF/PI aerogel with mass ratio of 3:1 was investigated and discussed in the following text. Moreover, the effect of nanofiber diameter on composite aerogel was also studied in this work. As shown in Fig. S5a and b, PVDF

nanofibers and PI nanofibers with average diameters of ~200, ~300 and ~400 nm were prepared by electrospinning, respectively. Then PVDF/PI aerogels were manufactured from these nanofibers and named as FP₂₀₀, FP₃₀₀, FP₄₀₀, respectively, in which “FP” refers to PVDF/PI aerogel and the subscript refers to the nanofiber diameter. As illustrated in Fig. S5c and d, FP₂₀₀, FP₃₀₀ and FP₄₀₀ show similar compression property and thermal conductivity. This is because that the mechanical properties mainly depend on the degree of crosslinking and entanglement of nanofibers, while the thermal conductivity generally decreases with increasing porosity, barely related to the size of nanofibers. Therefore, the diameter of nanofibers has almost little effect on the mechanical properties and thermal insulation properties of the resulting PVDF/PI aerogels.

Fig. 1b and c display SEM images of the PVDF/PI

aerogels. The cellular architecture shows a distinct open-cell geometry and the size of major cellular pores is about $80\ \mu\text{m}$ (Fig. 1b). Fig. 1c shows that the PVDF nanofibers and PI nanofibers are firmly interconnected to form a 3D network in which there are two ways of joining, i.e., chemical crosslinking and physical entanglement, with the former being the primary connection. The PVDF/PI aerogels have an attractive advantage of low density due to the large amount of air in the skeleton. As shown in Fig. 1d, the PVDF/PI aerogel with a density of $22.0\ \text{mg cm}^{-3}$ can be stably placed on top of the stamen without deforming it. The shapes of aerogels can be easily adjusted due to the simplicity of the preparing method and the facile availability of electrospun nanofibers. As shown in Fig. 1e, we can easily prepare aerogels with desired shapes, such as cones, cubes, triangular prisms and cylinders. Besides, the PVDF/PI aerogel exhibits excellent hydrophobicity. When dyed water droplets were

dripped on the surface of PVDF/PI aerogel, it was observed that the water droplets steadily stayed on the aerogel instead of penetrating into it (Fig. 1f). The superhydrophobic properties of the PVDF/PI aerogel enable it to display remarkable thermal insulating properties in high-temperature and humid environment (Fig. 1g).

PVDF has frequently been used to construct functional materials with excellent hydrophobic properties because of its rich fluorinated segments [37]. As illustrated in Fig. 2a, the water droplet on the surface of PVDF/PI aerogel maintained its round shape with a high contact angle of 152° and held 151° after 10 min, indicating its superhydrophobic property. When the superhydrophobic PVDF/PI aerogel was immersed in water by an external force, the surface of the aerogel was surrounded by the bubbles to present a silver mirror-like surface (Fig. 2b). Moreover, the as-prepared PVDF/PI aerogel can float easily on water, which can be ascribed to its super-

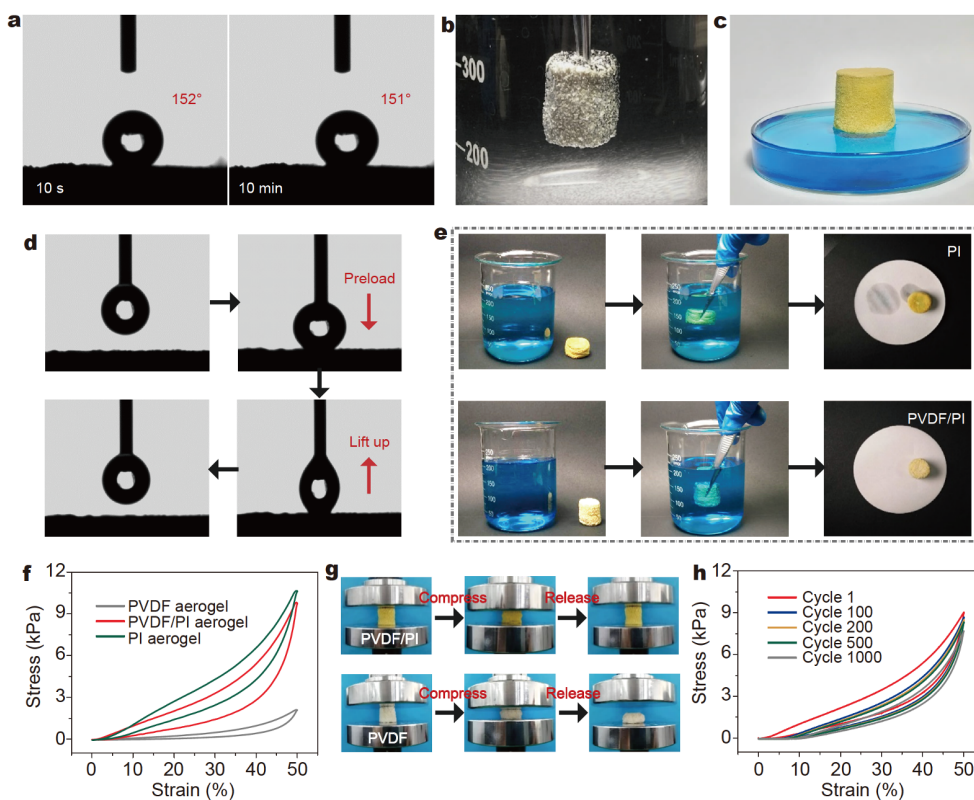


Figure 2 Hydrophobic and compressive performance of the PVDF/PI aerogel. (a) Water contact angles of the PVDF/PI aerogel taken at 10 s and 10 min. (b) The digital image of PVDF/PI aerogel immersed in water under the action of external force presents a silver mirror-like surface due to the surrounding bubbles. (c) The digital image of the PVDF/PI aerogel floated on water due to its superhydrophobicity and lightweight. (d) Photographs of the dynamic measurements of the water adhesion on the surface of PVDF/PI aerogel. (e) Comparison of hydrophobicity between PVDF/PI aerogel and PI aerogel. (f) Compressive stress-strain curves of the PVDF aerogel, PVDF/PI aerogel and PI aerogel at 50% strain. (g) Photographs of the PVDF/PI aerogel and PVDF aerogel under a compressing and releasing cycle ($\epsilon = 50\%$). (h) Fatigue test of the PVDF/PI aerogel at 50% strain for 1000 cycles.

hydrophobicity and lightweight (Fig. 2c). Except for superhydrophobicity, the resultant PVDF/PI aerogel also displays low adhesion to water. Even if the needle is preloaded, the water droplet did not spread out on the surface of PVDF/PI aerogel, which could be attributed to low adhesion between the specimen and the droplet (Fig. 2d). The process of continuous hydrophobicity is presented in Movie S1. The water droplets fall onto the aerogel and roll off rapidly, further indicating that the PVDF/PI aerogel equips outstanding hydrophobicity and low water adhesion. In comparison, pure PI aerogel has a water contact angle of only 75° (Fig. S6). We immersed both PI aerogel and PVDF/PI aerogel in water separately, stirred by external force, and then took them out on the filter paper. It can be seen that the PI aerogel leaves a large water trail on the filter paper, while the filter paper with the PVDF/PI aerogel is still dry (Fig. 2e and Movie S2). Moreover, the water contact angle achieved by the PVDF/PI aerogel is much higher than other hydrophobic materials including PAN/carbon nanotube/ Fe_3O_4 aerogel [6], nanocellulose aerogel [38], silica aerogel [39], konjac glucomannan-silica aerogel [40], clay/PVA aerogel [41], PVA/cellulose nanofibril aerogel [42] and hydroxyapatite nanowire aerogel [43] (Fig. S7). Besides the above intriguing superhydrophobic performance, the PVDF/PI aerogel also exhibits good mechanical properties, which are highly crucial for constructing thermal insulating materials. The mechanical properties of the PVDF aerogel, PVDF/PI aerogel and PI aerogel were also measured. As shown in Fig. 2f, both PVDF/PI aerogel and PI aerogel exhibit good compression resilience at 50% strain, while the compressive property of PVDF aerogel is relatively inferior. This can be explained that PI nanofibers with the conjugated structure of five-membered rings and six-membered rings show higher strength than that of PVDF nanofibers. Therefore, as mechanical support skeleton, PI nanofibers are sufficient to support the entire aerogel structure and enhance their structural stability after crosslinking by BA-a. Notably, the PVDF/PI aerogel can be reversibly compressed and released, showing a good compression property that is completely different from PVDF aerogel (Fig. 2g). The PVDF/PI aerogel can still be restored to its original shape after being compressed by a weight more than 2,000 times its own weight (Fig. S8). Furthermore, the PVDF/PI aerogel can bear 1,000 cyclic loading-unloading compression tests at a strain of 50% (Fig. 2h). Under cyclic compression test, the stress decay occurs mainly in the earlier period of the cycle and the structure becomes relatively stable in the subsequent cycles. This is because in the initial cycle, the composite

aerogel consumes energy from incompletely crosslinked nanofibers and unstable crosslinking points to counteract external forces, thereby keeping the overall structure of the aerogel stable. After 1000 cycles, the stress-strain curves are almost overlapped, demonstrating the excellent mechanical stability of the PVDF/PI aerogel.

Aerogel is one of the most outstanding thermal insulating materials with dramatically low thermal conductivity due to its high porosity [35]. The prepared PVDF/PI aerogel has high porosity (98.6%) and tortuous porous channels, which effectively reduce the thermal transportation of the gas and solid phases. As shown in Fig. 3a, compared with other commercial thermal insulating materials, the PVDF/PI aerogel owns a low thermal conductivity of $31.0 \text{ mW m}^{-1} \text{ K}^{-1}$ at room temperature. Due to the good thermal stability of PVDF/PI aerogel (stable even at 300°C in air atmosphere as shown in Fig. S9), it exhibits good thermal insulation performance in a wide temperature range from -60°C to 300°C . As shown in Fig. 3b, the thermal conductivity increases with the increasing temperature. However, thermal conductivity of the PVDF/PI aerogel is still only $58.2 \text{ mW m}^{-1} \text{ K}^{-1}$ even at 300°C . Herein, in order to explore the thermal insulation performance of the PVDF/PI aerogel in practical applications, we placed a PVDF/PI aerogel with a height of 15 mm on the hot stage with different temperatures or freezing copper billet to take thermal infrared images (illustrated in Fig. 3c). The temperature of the hot stage was set to 100, 200 and 300°C , respectively, and freezing copper billet was -30°C . Infrared thermal images of the PVDF/PI aerogel captured at 0, 1 and 5 min are presented. As displayed in Fig. 3d, when the heating time increased to 5 min, the detected surface temperatures of the PVDF/PI aerogel on -30 , 100, 200 and 300°C stage are only 6, 32, 41, and 55°C correspondingly, demonstrating its excellent thermal insulating properties at varied temperatures. The corresponding temperature-time curves are shown in Fig. 3e. As time goes on, the surface temperature of PVDF/PI aerogel is quite steady with little change, indicating an extraordinarily stable thermal insulation. In addition, their corresponding side thermal infrared images are shown in Fig. S10, further indicating excellent thermal insulating properties of the PVDF/PI aerogel. Significantly, compared with commercial PI foam, the PVDF/PI aerogel exhibits better thermal insulation properties, showing the broad prospects of the aerogels in practical applications (Fig. S11). Usually, thermal insulating materials are easily squeezed or vibrated under practical working conditions, which requires them to still have good thermal insulation

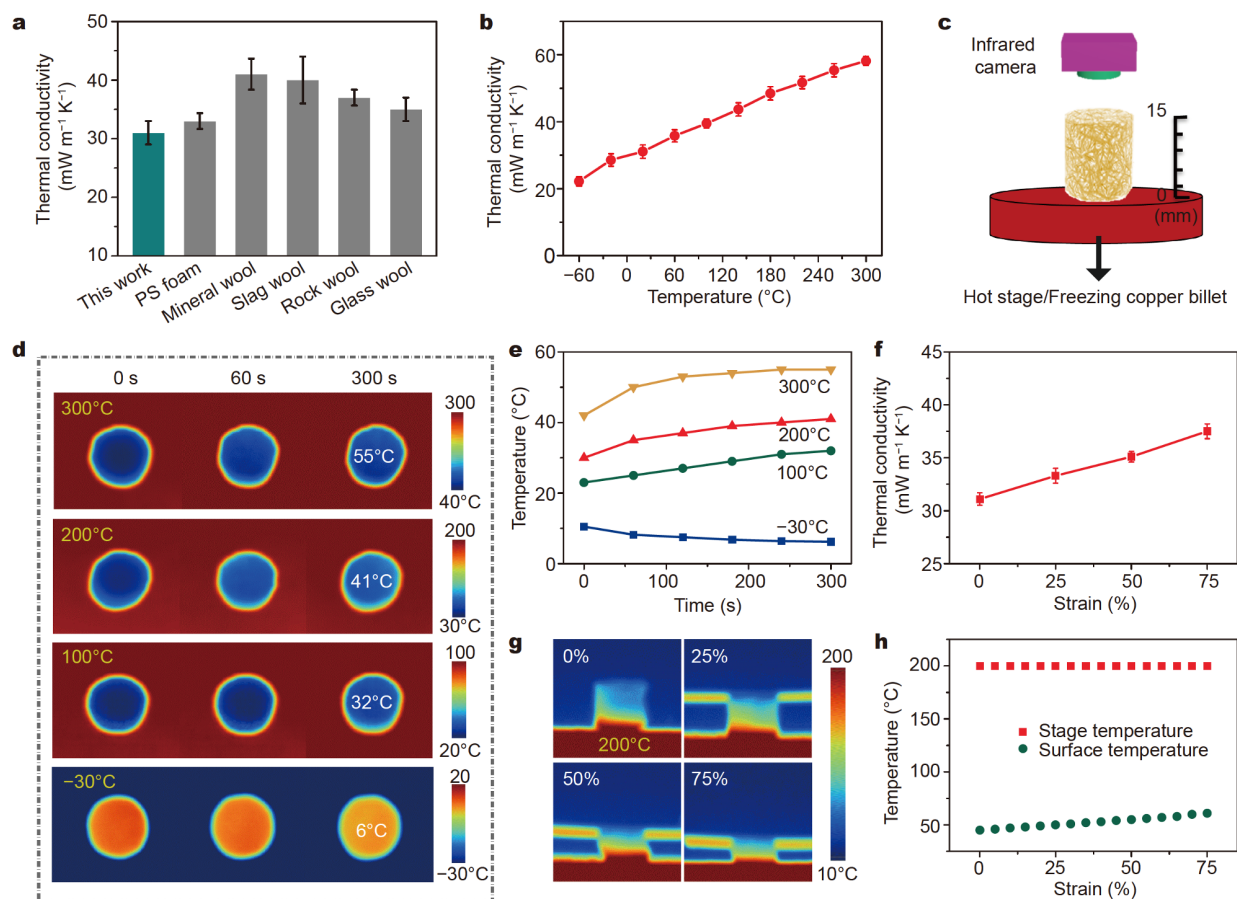


Figure 3 Thermal insulating properties of the PVDF/PI aerogel. (a) Thermal conductivity of PVDF/PI aerogel, PS foam, mineral wool, slag wool, rock wool and glass wool. (b) Thermal conductivity of the PVDF/PI aerogel with different temperatures. (c) Schematic diagram of the PVDF/PI aerogel placed on the hot stage. (d) Thermal infrared images of the PVDF/PI aerogel on hot stage or freezing copper billet for different time. (e) Variation of the temperature detected on the upper surface of the PVDF/PI aerogel with heating time. (f) Thermal conductivity of the PVDF/PI aerogel at different compressive strains. (g) Thermal infrared images of the PVDF/PI aerogel at different compressive strains on the hot stage. (h) Surface temperature of the PVDF/PI aerogel with different compressive strains on 200 $^{\circ}\text{C}$ hot stage. The error bars indicate standard deviations from five different samples in each case.

properties under deformation. The thermal conductivity of the PVDF/PI aerogel under different compressive strains is displayed in Fig. 3f. It can be seen that the PVDF/PI aerogel owns a low thermal conductivity of $37.5 \text{ mW m}^{-1} \text{K}^{-1}$ even at 75% strain, superior to some commercial insulating materials. The thermal infrared images and surface temperature curves of the PVDF/PI aerogel under different compression strains are also exhibited in Fig. 3g and h. As the compression strain increases, the temperature of upper surface of PVDF/PI aerogel only slightly increases, and the gap between surface temperature and the hot stage temperature (200 $^{\circ}\text{C}$) is approximately 139 $^{\circ}\text{C}$ at 75% strain. More relevant tests and temperature profiles for the PVDF/PI aerogel are shown in Fig. S12, indicating its excellent thermal in-

ulating performance under different temperatures and compressive strains, which makes the PVDF/PI aerogel an ideal thermal insulating material. In addition, the PVDF/PI aerogel is fire-retardant and can be self-extinguished after burning (Fig. S13), indicating its great potential as both thermal insulating and fire-resistant materials.

To further obtain insight into the thermal insulation of PVDF/PI aerogel in extremely humid environment, we measured its thermal conductivity at different temperatures and RH (Fig. 4a). The PVDF/PI aerogel displays low thermal conductivities of 43.5, 45.5, 46.7 and $48.6 \text{ mW m}^{-1} \text{K}^{-1}$ at 20, 40, 60 and 80 $^{\circ}\text{C}$ (100% RH), respectively. And it also possesses low thermal conductivities of 44.1, 45.7, 46.6, 48.2 and $48.6 \text{ mW m}^{-1} \text{K}^{-1}$

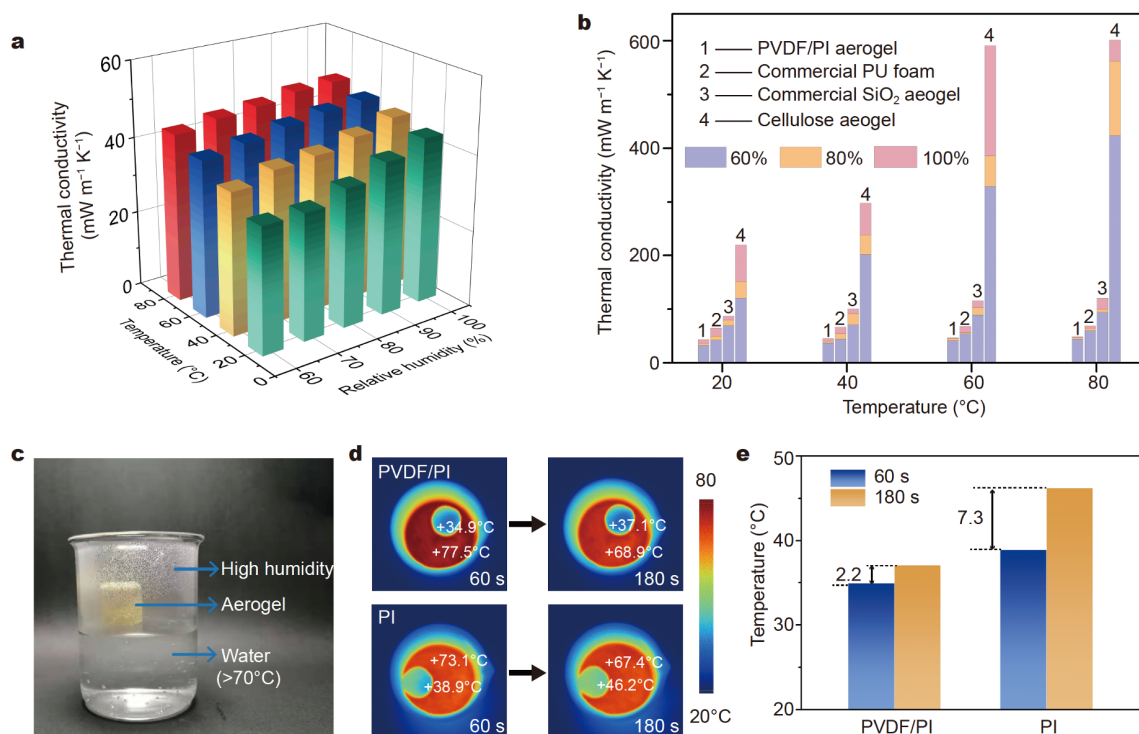


Figure 4 Thermal insulating properties of the PVDF/PI aerogel in extremely humid conditions. (a) Thermal conductivity of the PVDF/PI aerogel at different temperatures and RH. (b) Thermal conductivity of the PVDF/PI aerogel, commercial PU foam, commercial SiO₂ aerogel and cellulose aerogel at different temperatures and RH. (c) The PVDF/PI aerogel or PI aerogel in hot water. (d) Thermal infrared images of the PVDF/PI aerogel and PI aerogel in hot water. (e) Temperature change of the PVDF/PI aerogel and PI aerogel at 60 and 180 s.

at 60%, 70%, 80%, 90% and 100% RH (80°C), respectively. Although the thermal conductivity of PVDF/PI aerogel increases with temperature and humidity slightly, it still remains quite a low level (below 50 mW m⁻¹ K⁻¹) due to its hydrophobicity. Compared with other aerogel materials, the PVDF/PI aerogel shows much better thermal insulation performance in high humidity. As shown in Fig. 4b, cellulose aerogel has a high thermal conductivity of 423.3, 561.9 and 601.3 mW m⁻¹ K⁻¹ at 60%, 80% and 100% RH (80°C), respectively, due to its high hygroscopicity. Although SiO₂ aerogel has excellent thermal insulation properties in dry environment, it is difficult to maintain this performance in humid environment because of its poor moisture resistance. Commercial SiO₂ aerogel shows a thermal conductivity of 93.7, 99.4 and 120.5 mW m⁻¹ K⁻¹ at 60%, 80% and 100% RH (80°C), respectively. Similarly, commercial PU foam possesses a thermal conductivity of 60.1, 64.2 and 68.9 mW m⁻¹ K⁻¹ respectively in the same environment. This may be due to the fact that water gradually invades into the interior of the samples under high humidity, and water is a highly thermal conductive substance (thermal conductivity of

about 600 mW m⁻¹ K⁻¹), which will weaken the thermal insulation performance and even destroy the structure of the samples. However, the PVDF/PI aerogel exhibits a low thermal conductivity of only 48.6 mW m⁻¹ K⁻¹ even at 100% RH and 80°C, which can be attributed to the following two reasons. On one hand, the thermal conductivity of PVDF/PI aerogel only increases slightly with increasing temperature due to its good thermal insulation properties under a wide range of temperatures. On the other hand, on account of the excellent hydrophobicity and low water adhesion of PVDF/PI aerogel, water molecules are blocked and can hardly infiltrate into aerogels. A demonstration on the thermal insulation performance of PVDF/PI aerogel and PI aerogel at high humidity is shown in Fig. 4c. The two aerogels are placed into the water (>70°C) container in a high-humidity environment. Thermal infrared images indicate that the surface temperature of PVDF/PI aerogel is below 35°C and only increases by 2.2°C after 180 s, while that of PI aerogel increases by 7.3°C after 180 s (Fig. 4d and e), further indicating stable thermal insulating ability of the PVDF/PI aerogel at high humidity. Furthermore, as shown in

Fig. S14, the PVDF/PI aerogel possesses much lower thermal conductivity compared with other kinds of thermal insulating materials at different temperatures and RH, such as laterite rocks [44], aerogel-enhanced plaster [45], aerogel gypsum board [45], pure plaster [45], lightweight aggregate concrete [46], PU foam [47] and cement mortar [48]. These results support the employment of the superhydrophobic PVDF/PI aerogel as a superior thermal insulating material in high-temperature and humidity environment.

CONCLUSIONS

In summary, we have described a green and convenient route for the fabrication of superhydrophobic and compressible PVDF/PI nanofiber composite aerogel by the combination of electrospinning and freeze-drying method. PVDF and PI nanofibers are crosslinked together *via* BA-a to form a stable 3D network by heat treatment. The resultant PVDF/PI aerogel exhibits high porosity (98.6%), low density (22.0 mg cm^{-3}), good mechanical properties and low thermal conductivity ($31.0 \text{ mW m}^{-1} \text{ K}^{-1}$ at room temperature). More importantly, owing to its excellent thermal stability and superhydrophobicity with a water contact angle of 152° , the PVDF/PI aerogel possesses a low thermal conductivity of only $58.2 \text{ mW m}^{-1} \text{ K}^{-1}$ even at 300°C and $48.6 \text{ mW m}^{-1} \text{ K}^{-1}$ even at 100% RH, indicating its excellent thermal insulating ability in high-temperature and humidity environment, which is superior to many commercial insulating materials. Therefore, the PVDF/PI aerogels with prominent thermal insulation performance are highly promising to be used for building insulation materials, especially in extremely humid and hot environment.

Received 23 May 2020; accepted 10 September 2020;
published online 23 November 2020

- Chu S, Majumdar A. Opportunities and challenges for a sustainable energy future. *Nature*, 2012, 488: 294–303
- Schmidt DG. Research opportunities for future energy technologies. *ACS Energy Lett*, 2016, 1: 244–245
- Xu X, Zhang Q, Hao M, *et al.* Double-negative-index ceramic aerogels for thermal superinsulation. *Science*, 2019, 363: 723–727
- Hu F, Wu S, Sun Y. Hollow-structured materials for thermal insulation. *Adv Mater*, 2019, 31: 1801001
- Zhang L, Deng H, Fu Q. Recent progress on thermal conductive and electrical insulating polymer composites. *Compos Commun*, 2018, 8: 74–82
- Li Y, Liu X, Nie X, *et al.* Multifunctional organic-inorganic hybrid aerogel for self-cleaning, heat-insulating, and highly efficient microwave absorbing material. *Adv Funct Mater*, 2019, 29: 1807624
- Zhang J, Cheng Y, Tebyetekerwa M, *et al.* “Stiff-soft” binary synergistic aerogels with superflexibility and high thermal insulation performance. *Adv Funct Mater*, 2019, 29: 1806407
- Ibrahim M, Wurtz E, Biwole PH, *et al.* Hygrothermal performance of exterior walls covered with aerogel-based insulating rendering. *Energy Buildings*, 2014, 84: 241–251
- Kim NK, Kim K, Payne DA, *et al.* Fabrication of hollow silica aerogel spheres by a droplet generation method and sol-gel processing. *J Vacuum Sci Tech A-Vacuum Surf Films*, 1989, 7: 1181–1184
- Si Y, Wang X, Dou L, *et al.* Ultralight and fire-resistant ceramic nanofibrous aerogels with temperature-invariant superelasticity. *Sci Adv*, 2018, 4: eaas8925
- Zu G, Kanamori K, Wang X, *et al.* Superelastic triple-network polyorganosiloxane-based aerogels as transparent thermal superinsulators and efficient separators. *Chem Mater*, 2020, 32: 1595–1604
- Zhang X, Zhao X, Xue T, *et al.* Bidirectional anisotropic polyimide/bacterial cellulose aerogels by freeze-drying for super-thermal insulation. *Chem Eng J*, 2020, 385: 123963
- Guo H, Feng Q, Xu K, *et al.* Self-templated conversion of metallogel into heterostructured TMP@carbon quasiaerogels boosting bifunctional electrocatalysis. *Adv Funct Mater*, 2019, 29: 1903660
- Guo H, Zhou J, Li Q, *et al.* Emerging dual-channel transition-metal-oxide quasiaerogels by self-embedded templating. *Adv Funct Mater*, 2020, 30: 2000024
- Fu Y, Wang G, Mei T, *et al.* Accessible graphene aerogel for efficiently harvesting solar energy. *ACS Sustain Chem Eng*, 2017, 5: 4665–4671
- Hu H, Zhao Z, Wan W, *et al.* Ultralight and highly compressible graphene aerogels. *Adv Mater*, 2013, 25: 2219–2223
- Chen B, Bi H, Ma Q, *et al.* Preparation of graphene-MoS₂ hybrid aerogels as multifunctional sorbents for water remediation. *Sci China Mater*, 2017, 60: 1102–1108
- Wong JCH, Kaymak H, Brunner S, *et al.* Mechanical properties of monolithic silica aerogels made from polyethoxydisiloxanes. *Microporous Mesoporous Mater*, 2014, 183: 23–29
- Sun X, Wei Y, Li J, *et al.* Ultralight conducting PEDOT:PSS/carbon nanotube aerogels doped with silver for thermoelectric materials. *Sci China Mater*, 2017, 60: 159–166
- Mu P, Zhang Z, Bai W, *et al.* Superwetting monolithic hollow-carbon-nanotubes aerogels with hierarchically nanoporous structure for efficient solar steam generation. *Adv Energy Mater*, 2019, 9: 1802158
- Baskakov SA, Baskakova YV, Kabachkov EN, *et al.* Novel superhydrophobic aerogel on the base of polytetrafluoroethylene. *ACS Appl Mater Interfaces*, 2019, 11: 32517–32522
- Diascorn N, Calas S, Sallée H, *et al.* Polyurethane aerogels synthesis for thermal insulation—textural, thermal and mechanical properties. *J Supercritical Fluids*, 2015, 106: 76–84
- Du A, Wang H, Zhou B, *et al.* Multifunctional silica nanotube aerogels inspired by polar bear hair for light management and thermal insulation. *Chem Mater*, 2018, 30: 6849–6857
- Cahn RW. Strategies to defeat brittleness. *Nature*, 1988, 332: 112–113
- Si Y, Yu J, Tang X, *et al.* Ultralight nanofibre-assembled cellular aerogels with superelasticity and multifunctionality. *Nat Commun*, 2014, 5: 5802
- Liu Z, Lyu J, Fang D, *et al.* Nanofibrous Kevlar aerogel threads for thermal insulation in harsh environments. *ACS Nano*, 2019, 13: 5703–5711
- Qian Z, Yang M, Li R, *et al.* Fire-resistant, ultralight, superelastic

- and thermally insulated polybenzazole aerogels. *J Mater Chem A*, 2018, 6: 20769–20777
- 28 Cranford SW, Tarakanova A, Pugno NM, *et al.* Nonlinear material behaviour of spider silk yields robust webs. *Nature*, 2012, 482: 72–76
- 29 Ding Y, Hou H, Zhao Y, *et al.* Electrospun polyimide nanofibers and their applications. *Prog Polym Sci*, 2016, 61: 67–103
- 30 Xue J, Wu T, Dai Y, *et al.* Electrospinning and electrospun nanofibers: methods, materials, and applications. *Chem Rev*, 2019, 119: 5298–5415
- 31 Tian J, Shi Y, Fan W, *et al.* Ditungsten carbide nanoparticles embedded in electrospun carbon nanofiber membranes as flexible and high-performance supercapacitor electrodes. *Compos Commun*, 2019, 12: 21–25
- 32 Zhu J, Lv S, Yang T, *et al.* Facile and green strategy for designing ultralight, flexible, and multifunctional PVA nanofiber-based aerogels. *Adv Sustain Syst*, 2020, 4: 1900141
- 33 Li Y, Cao L, Yin X, *et al.* Semi-interpenetrating polymer network biomimetic structure enables superelastic and thermostable nanofibrous aerogels for cascade filtration of PM_{2.5}. *Adv Funct Mater*, 2020, 30: 1910426
- 34 Qian Z, Wang Z, Chen Y, *et al.* Superelastic and ultralight polyimide aerogels as thermal insulators and particulate air filters. *J Mater Chem A*, 2018, 6: 828–832
- 35 Jiang S, Uch B, Agarwal S, *et al.* Ultralight, thermally insulating, compressible polyimide fiber assembled sponges. *ACS Appl Mater Interfaces*, 2017, 9: 32308–32315
- 36 Fan W, Zhang X, Zhang Y, *et al.* Lightweight, strong, and superthermal insulating polyimide composite aerogels under high temperature. *Compos Sci Tech*, 2019, 173: 47–52
- 37 Li X, Yu X, Cheng C, *et al.* Electrospun superhydrophobic organic/inorganic composite nanofibrous membranes for membrane distillation. *ACS Appl Mater Interfaces*, 2015, 7: 21919–21930
- 38 de Oliveira PB, Godinho M, Zattera AJ. Oils sorption on hydrophobic nanocellulose aerogel obtained from the wood furniture industry waste. *Cellulose*, 2018, 25: 3105–3119
- 39 Zhao Y, Li Y, Zhang R. Silica aerogels having high flexibility and hydrophobicity prepared by sol-gel method. *Ceramics Int*, 2018, 44: 21262–21268
- 40 Zhu J, Hu J, Jiang C, *et al.* Ultralight, hydrophobic, monolithic konjac glucomannan-silica composite aerogel with thermal insulation and mechanical properties. *Carbohydrate Polym*, 2019, 207: 246–255
- 41 Madyan OA, Fan M. Hydrophobic clay aerogel composites through the implantation of environmentally friendly water-repellent agents. *Macromolecules*, 2018, 51: 10113–10120
- 42 Zhang X, Wang H, Cai Z, *et al.* Highly compressible and hydrophobic anisotropic aerogels for selective oil/organic solvent absorption. *ACS Sustain Chem Eng*, 2018, 7: 332–340
- 43 Zhang YG, Zhu YJ, Xiong ZC, *et al.* Bioinspired ultralight inorganic aerogel for highly efficient air filtration and oil–water separation. *ACS Appl Mater Interfaces*, 2018, 10: 13019–13027
- 44 Shaik S, Talanki Puttaranga Setty AB. Influence of ambient air relative humidity and temperature on thermal properties and unsteady thermal response characteristics of laterite wall houses. *Building Environ*, 2016, 99: 170–183
- 45 Nosrati RH, Berardi U. Hygrothermal characteristics of aerogel-enhanced insulating materials under different humidity and temperature conditions. *Energy Buildings*, 2018, 158: 698–711
- 46 Nguyen LH, Beaucour AL, Ortola S, *et al.* Experimental study on the thermal properties of lightweight aggregate concretes at different moisture contents and ambient temperatures. *Construction Building Mater*, 2017, 151: 720–731
- 47 Alvey JB, Patel J, Stephenson LD. Experimental study on the effects of humidity and temperature on aerogel composite and foam insulations. *Energy Buildings*, 2017, 144: 358–371
- 48 Siwińska A, Garbalińska H. Thermal conductivity coefficient of cement-based mortars as air relative humidity function. *Heat Mass Transfer*, 2011, 47: 1077–1087

Acknowledgements The authors are grateful for the financial support from the National Natural Science Foundation of China (21674019 and 21704014), the Fundamental Research Funds for the Central Universities (2232019A3-03), the Graduate Student Innovation Fund of Donghua University (CUSF-DH-D-2019006), Shanghai Sailing Program (17YF1400200), Shanghai Municipal Education Commission (17CG33), and the Ministry of Education of the People's Republic of China (6141A0202202).

Author contributions Yang F contributed to the methodology and investigation, and wrote the paper. Zhao X guided the mechanical measurements and contributed to the theoretical analysis. Xue T guided the FT-IR and DSC measurements. Xue T and Yuan S participated in the discussion. Huang Y contributed to the schematic diagrams part. Fan W contributed to the conceptualization, supervision and editing. Liu T contributed to the supervision and editing.

Conflict of interest The authors declare no conflict of interest.

Supplementary information Experimental details and supporting data are available in the online version of the paper.



Fan Yang is a master student of the College of Materials Science and Engineering, Donghua University. She joined Prof. Tianxi Liu's group in 2018 and her research interest is focused on the preparation and properties of nanofiber aerogel materials.



Wei Fan is an associate professor of the College of Materials Science and Engineering, Donghua University. She received her PhD degree in macromolecular chemistry and physics from Fudan University in 2015. Her research interests include functional aerogel composites, polymer nanocomposites and electrochemical energy storage materials.



Tianxi Liu is a professor of the College of Materials Science and Engineering, Donghua University. He received his PhD degree from Changchun Institute of Applied Chemistry, Chinese Academy of Sciences in 1998. His research interests include polymer nanocomposites, new energy materials and devices, hybrid materials, nanofibers and their composite materials.

极端湿热环境下隔热的超疏水聚偏氟乙烯/聚酰亚胺纳米纤维复合气凝胶

杨帆¹, 赵兴宇¹, 薛甜甜¹, 元诗佳¹, 黄云鹏², 樊玮^{1*}, 刘天西^{1,2*}

摘要 优异的隔热材料在建筑、航空航天和体育设备等领域有着广泛的应用需求. 然而, 在实际应用中, 隔热材料在不同温度和湿度条件下, 其性能往往会恶化. 因此, 构建在极端湿热环境下仍具有出色的隔热性能的块状材料是非常重要的. 在本工作中, 我们构思了一种绿色制备策略, 即通过静电纺丝和冷冻干燥技术来制备超疏水且可压缩的聚偏氟乙烯/聚酰亚胺(PVDF/PI)纳米纤维复合气凝胶. PVDF纳米纤维和PI纳米纤维分别充当疏水性纤维骨架和机械支撑骨架, 形成具有良好机械柔韧性的坚固的三维框架. PVDF/PI气凝胶在室温下具有出色的超疏水特性(水接触角为 152°)和低导热性($31.0 \text{ mW m}^{-1} \text{ K}^{-1}$). 同时, 在100%湿度(80°C)下, PVDF/PI气凝胶仅显示出 $48.6 \text{ mW m}^{-1} \text{ K}^{-1}$ 的低热导率, 其性能优于大多数商业绝热材料. 因此, 新型的PVDF/PI复合气凝胶有望成为高温和高湿环境中应用的优良隔热材料.